Transverse seismic response of continuous steel-concrete composite bridges exhibiting dual load path

E. Tubaldi[1], M. Barbato[2*] and A. Dall'Asta[3]

[1]*DACS, Dipartimento di Architettura Costruzione e Strutture, Università Politecnica delle Marche, Via Brecce Bianche, 60131, Ancona, Italy*
[2]*Department of Civil & Environmental Engineering, Louisiana State University and A&M College, 3531 Patrick F. Taylor Hall, Nicholson Extension, Baton Rouge, Louisiana 70803, USA*
[3]*Dipartimento di Progettazione e Costruzione dell'Ambiente, University of Camerino, Viale della Rimembranza, 63100, Ascoli Piceno (AP), Italy*

(Received December 1, 2009, Accepted February 8, 2010)

Abstract. Multi-span steel-concrete composite (SCC) bridges are very sensitive to earthquake loading. Extensive damage may occur not only in the substructures (piers), which are expected to yield, but also in the other components (e.g., deck, abutments) involved in carrying the seismic loads. Current seismic codes allow the design of regular bridges by means of linear elastic analysis based on inelastic design spectra. In bridges with superstructure transverse motion restrained at the abutments, a dual load path behavior is observed. The sequential yielding of the piers can lead to a substantial change in the stiffness distribution. Thus, force distributions and displacement demand can significantly differ from linear elastic analysis predictions. The objectives of this study are assessing the influence of piers-deck stiffness ratio and of soil-structure interaction effects on the seismic behavior of continuous SCC bridges with dual load path, and evaluating the suitability of linear elastic analysis in predicting the actual seismic behavior of these bridges. Parametric analysis results are presented and discussed for a common bridge typology. The response dependence on the parameters is studied by nonlinear multi-record incremental dynamic analysis (IDA). Comparisons are made with linear time history analysis results. The results presented suggest that simplified linear elastic analysis based on inelastic design spectra could produce very inaccurate estimates of the structural behavior of SCC bridges with dual load path.

Keywords: steel-concrete composite structures; bridges; nonlinear finite element method; soil-structure interaction; seismic behavior; incremental dynamic analysis.

1. Introduction

The damage produced by recent seismic events all over the world has shown that steel-concrete composite (SCC) bridge structures are very sensitive to earthquake loading (Astaneh-Asl *et al.* 1994, Itani *et al.* 2004, Kawashima 2007). Current seismic design codes for bridges allow the formation of plastic hinges at the base of the piers during severe shaking in order to reduce the design seismic forces. Other structural members such as deck, bearing devices, abutments and foundations must be designed to remain elastic in order to avoid brittle failure. The unsatisfactory

* Corresponding author, Assistant Professor, E-mail: mbarbato@lsu.edu

performance of several multi-span SCC bridges in recent earthquakes has shown that extensive damage can occur not only in the substructures, which are expected to yield, but also in the components of the superstructure involved in carrying the seismic loads (Itani *et al.* 2004). Thus, accurate evaluation of the actual forces and displacement demands for every bridge structural component is crucial to ensure the desired structural behavior.

In order to reduce deck bending and to avoid expensive bi-directional joints, a rigid connection can be realized between the deck and the abutments by means of fixed bearings or special links restraining the transverse displacements (ECS 2005). In this situation, the sequential yielding of the piers can cause a modification of the structural behavior in the post-yielding response. These bridge configurations with abutment restraints are commonly referred to as bridges with "dual (elastic and inelastic) load paths" (Calvi 2004). In fact, only a portion of the inertia forces developed in the deck is transmitted to the pier footings by column bending, while the remaining part is transmitted to the abutments by superstructure bending. The transfer mechanism involving the piers is referred to as the inelastic path, since the piers are expected to yield in order to dissipate energy. The second mechanism, involving deck bending and abutments reactions, is denoted as the elastic path because these structural components are designed to remain elastic. For low values of the seismic intensity, the portion of load carried by each path strongly depends on the relative column-to-deck stiffness ratio as well as on the degree of lateral restraint provided at the abutments. However, for increasing values of the seismic intensity, piers yield and the additional seismic demand must be completely absorbed by the deck-abutments system (Calvi 2004). This different load transfer mechanism can cause two major problems. On one hand, the abutment reactions and the deck transverse bending moments can increase, even more than proportionally, after yielding of the piers, and thus their critical values can be rapidly attained. On the other hand, the maximum deformation capacity of the deck, which is designed to remain elastic, may be attained. In this situation, deck yielding (which is undesirable in a capacity design context) limits the pier plastic strains and consequently the global dissipation capacity of the entire structural system. Despite of such complex post-elastic behavior, linear elastic analysis based on inelastic design spectra (ECS 2005, Kolias 2008) is nowadays the most popular method used, for design purposes, to predict the behavior of bridges subjected to earthquake ground motions acting along the bridge transverse direction. Several studies on seismic transverse behavior of continuous bridges highlight the limits of linear elastic analysis based on response spectra (Calvi 2004, Benzoni *et al.* 2003, Lessloss 2007), while only few studies investigate the consequences of limited strength and deformability of the deck on the global behavior and the relevant modeling problems (Itani *et al.* 2004, Lessloss 2007, Panagiotakos *et al.* 2006).

The present study investigates in detail the transverse behavior of a specific bridge typology consisting of a continuous SCC deck with transverse restraints at the abutments. Particular attention is given to the effects of the dual load path behavior on the abutment reactions, the deck bending and the curvature demand at the base of the piers. This study considers as benchmark example a three-span SCC bridge, which is representative of numerous medium-span existing bridges (Calgaro 1994, Dezi 2008). Based on nonlinear finite element (FE) multi-record incremental dynamic analysis (IDA) (Vamvatsikos and Cornell 2002), a parametric analysis is carried out to evaluate the sensitivity of seismic response and collapse modalities on deck-piers stiffness ratio, which is the parameter that influences the most the bridge response. The dynamic soil-structure interaction (SSI) effects are also taken into account by considering four different ground types which represent a wide range of local soil conditions. Nonlinear FE IDAs are performed for increasing intensities of the ground motions until the bridges reach failure, defined as the reaching of the ultimate curvature

capacity of the piers' base or of the yield curvature in the deck (ECS 2005), whichever happens first. The seismic input is described by four different sets, each consisting of 22 natural accelerograms and chosen to represent the ground motions likely to happen for the different ground types considered. It is noteworthy that other geometrical and mechanical parameters as well as the bridge typology can influence the global behavior of dual load path bridges. However, most of these parameters, such as span lengths and deck width, are mainly determined by economical and traffic flow considerations and do not show large variation in real applications of SCC bridges. Therefore, geometrical and mechanical parameters other than pier/deck stiffness ratio and local soil condition are not included in this parametric study.

Changes in the failure mechanisms are highlighted together with the evolution of critical engineering demand parameters for increasing intensities of the seismic input. Furthermore, results obtained through nonlinear FE analyses are compared with those obtained from linear elastic analyses in order to assess the effectiveness and/or highlight the limits of design methods based on elastic analysis combined with inelastic design spectra.

2. Case study and parametric analysis

The bridges considered as benchmarks in this paper have a total length of 130 m divided into three spans with lengths L_1 = 40 m, L_2 = 50 m and L_3 = 40 m, respectively (Fig. 1).

The superstructure is designed according to the Eurocodes in function of the non-seismic load combinations and consists of a reinforced concrete slab of width equal to 12 m, which can host two traffic lanes, and of two steel girders positioned symmetrically with respect to the deck centerline and at a distance of 6 m between their centerlines (Dezi and Formica 2006). Fig. 2(a) shows a typical transverse section of the deck. Details of the steel girders are depicted in Fig. 2(b), where the thicknesses of the flanges and web are provided for the five different girder cross-sections used along the deck axis and denoted as *S*1 through *S*5 in the same figure. The deck slab is haunched and the thickness varies between 200 mm and 350 mm. The longitudinal reinforcement is equal to 2% of the slab area at supports (hogging regions) and to 1% at midspans (sagging regions). The distributed dead load due to self-weigh of the structural and non-structural elements permanently connected to the bridge is equal to 138 kN/m (Dezi and Formica 2006). The deck is transversely fixed at the abutments. The support to the deck is provided by two reinforced concrete piers with a circular cross-section of diameter D = 1.8 m.

In the parametric analysis, the piers aspect ratio H/D between columns height H and cross-section diameter D has been chosen as the parameter representing the pier-to-deck relative stiffness. This choice allows reducing significantly the number of analyses required if both H and D were used as

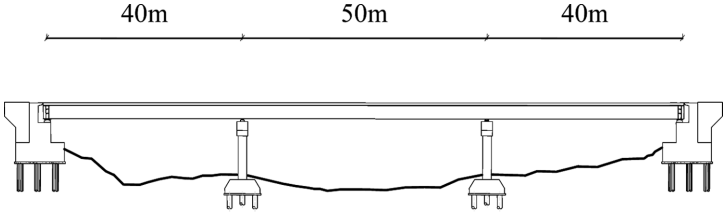

Fig. 1 Bridge longitudinal profile

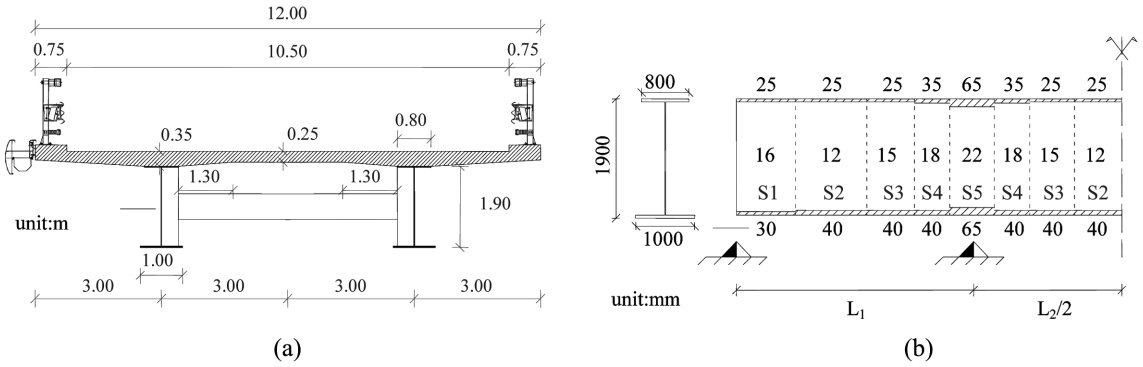

Fig. 2 Bridge deck cross-section properties: (a) typical deck transverse section, (b) girder cross-section geometry

independent parameters. The ratio H/D is varied from 3.0 to 9.0 with unit increments (i.e., H = 5.4 m, 7.2 m, 9.0 m, 10.8 m, 12.6 m, 14.4 m and 16.2 m) in order to investigate the influence of the pier stiffness and pier resisting forces on the global bridge response. Smaller heights of the piers are not considered since, for $H/D < 3$, the shear behavior would prevail on the flexural behavior. Higher pier heights (i.e., $H/D > 9$) are also not considered because a hollow section would usually be preferred as a design solution in order to reduce the pier mass. The circular columns have a fixed longitudinal reinforcement ratio equal to 1% of the concrete area. Transverse reinforcement with a volumetric ratio ρ_w= 0.5% is provided in the hinge regions with the aim of confining the concrete and preventing premature shear failure. Concrete belonging to class C30/37 (with mean compressive strength equal to 38 MPa) and C35/45 (with mean compressive strength equal to 43 MPa) is used for the piers and the superstructure slab, respectively. The reinforcement bars are made of grade B450C steel (with characteristic yield strength of 450 MPa), while the deck girders are made of grade S355 steel (with characteristic yield strength of 355 MPa).

3. Finite element models of the structural systems

Two sets of linear elastic and nonlinear hysteretic FE models of the considered structural systems are built in order to simulate the structural behavior and compare the simulation results produced by the two analysis methodologies. In both FE model sets, the superstructure (deck) is modeled using linear elastic three-dimensional Timoshenko frame elements. An effective stiffness, smaller than the initial tangent stiffness (gross flexural stiffness), is adopted to represent the transverse behavior of the deck and approximately account for the slab cracking. The reduction of the gross flexural stiffness is determined by using an ad-hoc moment-curvature analysis program which is also used to estimate the yield moments and curvatures (Caltrans 2006). It is noteworthy that appropriate finite elements are available to model rigorously the hysteretic behavior at the material level and the connection deformability of SCC beams (Dall'Asta and Zona 2002, Zona *et al*. 2008). Nevertheless, since the superstructure is not expected to yield (i.e., the nonlinear behavior is very limited) (ECS 2005), the simplifying modeling solution described above is preferred to drastically reduce the computational cost of the numerous time history analyses performed for this study.

The deck moment capacity is evaluated according to Eurocode 8-Part 2 (ECS 2005), which defines the strain limits under transverse seismic action. Fig. 3 plots the moment-curvature diagrams

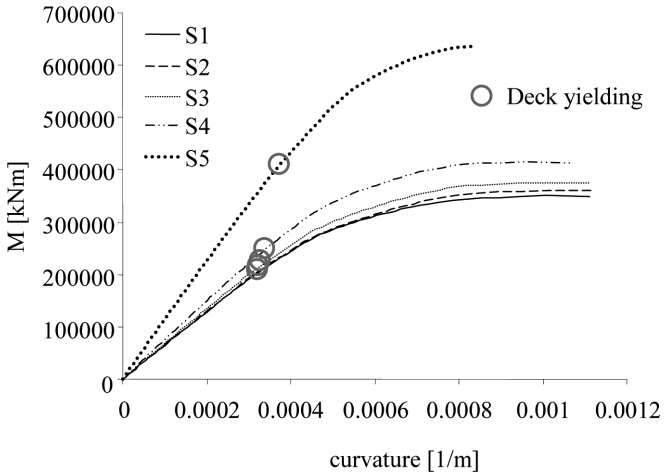

Fig. 3 Transverse moment-curvature diagrams for the different superstructure cross-sections (S1 through S5)

in the transverse direction, for the different cross-sections shown in Fig. 2(b). The moment-curvature relationships have been determined assuming that the influence of the bending moments acting along the longitudinal direction of the bridge is negligible (i.e., three-dimensional moment interaction is neglected). Due to the variation of the girder cross-section geometry, also the deck yield moments under transverse deformation are not constant along the longitudinal axis. In contrast, a small variability is observed in the values of the deck yield curvature μ_{max}, since μ_{max} is mainly influenced by the deck width B and by the reinforcement yield strain ε_{sy}, which remain constant along the bridge.

In the nonlinear hysteretic models, the piers are modeled using the three-dimensional frame element with inelastic hinges developed by Scott and Fenves (2006). This frame element is based on the flexibility formulation and a lumped plasticity model according to which the plastic deformations are concentrated over a specified hinge length at the element ends. Nonlinear axial force and bending moment interaction is accounted for through a fiber-section integration of the cross-section stress resultants. The remaining portion of the element is modeled as linear elastic. The axis of the element is taken as the straight line connecting the geometrical centers of the columns and the cap beams. A rigid end zone (1.81 m in length) is located at the top of the columns in order to account for the offset between the centerline of the cap beam and of the deck. The plastic hinge length at the base of the pier, L_p, is estimated following the Eurocode 8-Part 2 (ECS 2005) as

$$L_p = 0.10 \cdot L + 0.015 \cdot f_{yk} \cdot d_s \tag{1}$$

in which f_{yk} = characteristic yield stress of reinforcement steel, d_s = diameter of longitudinal rebars, and L = distance between the plastic hinge and the section of zero moment. The length of the plastic hinge zone at the top of the piers is assumed equal to zero since the connection between the top of the piers and the superstructure is not monolithic and plastic hinges are expected to form only at the pier bases. The effect of confinement on the concrete core in the plastic hinge zone is taken into account according to Appendix E of Eurocode 8-Part 2 (ECS 2005), which is based on the Mander's model (Mander *et al.* 1988). The core concrete compressive strength increases from

38000 kN/m^2 to 45879 kN/m^2 and the ultimate deformation increases from 0.0035 to 0.0097, due to confinement. The concrete stress-strain relationship is modeled through the Kent-Park model (Kent and Park 1971). Degrading of stiffness in linear unloading/reloading is modeled according to Karsan and Jirsa (1969). The reinforcement steel is modeled by the Menegotto-Pinto constitutive model (Menegotto and Pinto 1973), with yield strength f_y = 517.5 MPa, Young's modulus E = 210000 MPa and hardening ratio b = 0.0086. The effective stiffness characterizing the elastic part of the frame elements modeling the piers is determined from the yield moment M_y and the yield curvature φ_y (Calvi 2004, Priestley *et al.* 2007)

$$EI_{eff} = \frac{M_y}{\varphi_y} \tag{2}$$

In the linear elastic models, elastic frame elements are adopted for both deck and piers. The linear elastic frame elements used to model the piers are characterized by an effective stiffness estimated from moment-curvature analysis (Calvi 2004, Priestley *et al.* 2007, Caltrans 2006, ECS 2005), similarly as for the linear elastic portions in the nonlinear hysteretic models.

Linear and nonlinear FE time history response analyses are performed with the support of the FE software OpenSees (McKenna *et al.* 2006). A 2% Rayleigh damping matrix is assumed based on the periods of the two modes (i.e., first and third modes of vibration) with the highest participating mass ratio, identified through modal analysis. These two modes of vibration are particularly important in the description of the seismic transverse behavior. In fact, the first mode of vibration is characterized by a participating mass ratio higher than 75%, while the third mode of vibration influences significantly the abutment reactions. The Rayleigh damping matrix is updated at each time-step using the model tangent stiffness matrix (Priestley *et al.* 2007). Time-step integration is performed using the unconditionally stable constant acceleration Newmark-β scheme (Chopra 2001).

4. Modeling of soil-structure interaction

For the considered benchmark example, the SSI is modeled using the sub-domain approach (Wolf 1985). The foundations of piers and abutments are the same for all models and consist of pile groups (3×3 for piers and 4×3 for abutments) embedded in uniform soil. The piles have length L_{pile} = 20 m, diameter D_{pile} = 1000 mm and spacing $s_{pile} = 3D_{pile}$. The impedance parameters are determined by means of a FE-based model recently proposed in Dezi *et al.* (2009). Four different local soil conditions are considered, representing the A, B, C and D ground types as classified in both the Eurocode (ECS 2005) and the USGS classification (PEER 2006). For each ground type, different values of the shear wave velocity, V_s, and Young's modulus, E_s, are assumed as shown in Table 1, where the values assumed for the soil density, ρ_s, and the soil damping ratio, ξ_s, are also provided.

Table 1 Ground types

ground type	V_s [m/s]	E_s [kN/m^2]	ρ_s [Mg/m^3]	ξ_s
A	>800	-	-	-
B	650	1764000	1.75	10%
C	300	403200	1.6	10%
D	150	94500	1.5	10%

Table 2 Impedance matrix relative to pier foundations for the model with H/D = 3 (ground type B)

	y	r_x	r_z	z
K_y [kN/m]	9.0E+06	-7.7E+06	0	0
C_y [kNs/m]	1.5E+05	-8.4E+04	0	0
K_{rx} [kNm/rad]		2.8E+08	0	0
C_{rx} [kNms/rad]		2.1E+06	0	0
K_{rz} [kNm/rad]	sym		3.1E+08	0
C_{rz} [kNms/rad]			2.8E+06	0
K_z [kN/m]				2.2E+07
C_z [kNs/m]				2.9E+05

Table 3 Impedance matrix relative to abutment foundations for the model with H/D = 3 (ground type B)

	y	r_x	r_z	z
K_y [kN/m]	1.04E+07	-9.3E+06	0	0
C_y [kNs/m]	1.8E+05	-1.0E+05	0	0
K_{rx} [kNm/rad]		6.1E+08	0	0
C_{rx} [kNms/rad]		4.2E+06	0	0
K_{rz} [kNm/rad]	sym		5.2E+08	0
C_{rz} [kNms/rad]			4.3E+06	0
K_z [kN/m]				2.6E+07
C_z [kNs/m]				3.8E+05

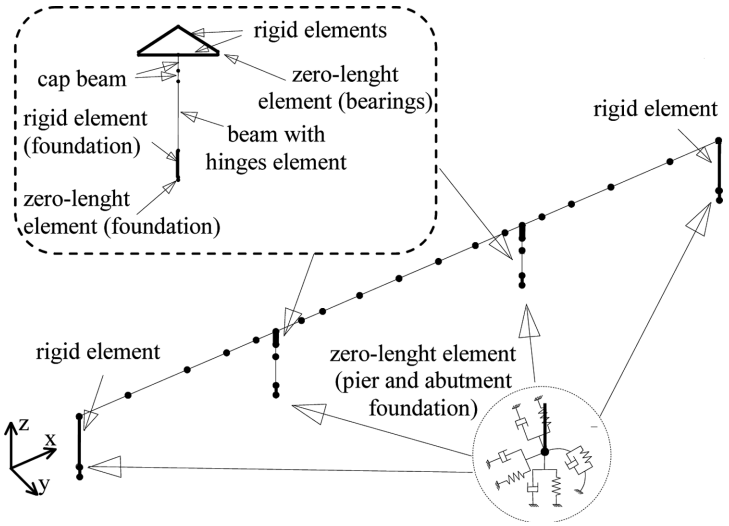

Fig. 4 Finite element model of an analyzed bridge accounting for SSI

The foundations impedance values adopted in the FE analyses are evaluated at the frequency of the first transverse mode. Tables 2 and 3 provide the impedance matrices for the transverse behavior corresponding to T = 0.623s (case H/D = 3, ground type B). The x-axis coincides with the longitudinal axis of the deck, the y-axis is transversely oriented and the z-axis is vertical. The symbols r_x and r_z denote the rotations about the axis x and z, respectively. The impedance matrices

used in this study for all four ground types can be found in (Tubaldi *et al.* 2009). The participating soil mass at the abutments is estimated based on the critical length of the embankment and evaluated through the formula proposed by Zhang and Makris (Aviram *et al.* 2008, Zhang and Makris 2002).

Fig. 4 illustrates the finite element model of the bridge corresponding to $H/D = 4$ accounting for soil-structure interaction effects at the base of piers and abutments.

5. Incremental dynamic analysis procedure and ground motion selection

Incremental Dynamic Analysis (IDA) (Vamvatsikos and Cornell 2002) is a well-known and widely used parametric method of analysis for estimating the dynamic response of a structure under seismic excitation. A single-record IDA consists in repeatedly subjecting a FE structural model to a ground motion record scaled by gradually increasing its intensity. It can be regarded as an extension of the concept of pushover analysis from the static to the dynamic case, since requires scaling the intensity of the record rather than a certain distribution of forces. The typical result of a single-record IDA is a single-record IDA curve, which is the plot of a structural response quantity of interest (Engineering Demand Parameter, *EDP*), observed or deduced from a nonlinear dynamic analysis, versus a properly chosen Intensity Measure (*IM*). In the case of bridges, *EDP*s can be classified in three groups (Mackie and Stojadinovic 2005), (1) global *EDP*s, which describe the overall bridge response, such as maximum column displacement, motion at the abutments, and residual displacements; (2) intermediate *EDP*s, which describe the bridge structural components performance, such as maximum column curvature demand and forces transmitted to the abutments; and (3) local *EDP*s, which describe structural components response at material level, such as maximum stresses and strains. Another useful result of a single-record IDA is the so called "dynamic pushover" curve (Mwafy and Elnashai 2001), e.g., for a frame structure, the plot of the maximum base shear experienced during the time history for increasing *IM* values versus the maximum displacement of a control node.

A multi-record IDA is defined as the collection of several single-record IDAs in which the same structural model is subjected to different ground motion records. The typical result of a multi-record IDA is an IDA curve set, which can be synthesized by the statistical properties (e.g., mean and coefficient of variation, COV) of the obtained population of IDA curves. Multi-record IDAs are employed to estimate the uncertainties of the *EDP*s due to the record-to-record variability (Vamvatsikos and Cornell 2002).

A crucial aspect of IDA is the choice of an appropriate *IM*, which must be efficient (i.e., it minimizes the dispersion/COV of the *EDP*) and sufficient (i.e., the *EDP* is function only of the *IM*) (Shome *et al.* 1998). For a structure whose behavior is regular and dominated by its first mode of vibration, the pseudo-spectral acceleration, $S_a(T_1, \xi)$, computed for the first period of vibration T_1 and for the equivalent viscous damping ξ of the model, has proven to be a very good *IM* (Vamvatsikos and Cornell 2002, Shome *et al.* 1998). The bridges analyzed in this study are characterized by a regular geometry and their response is dominated by their first mode of vibration. Thus, the pseudo-spectral acceleration $S_a(T_1, \xi)$ is assumed here as *IM*. In order to use this *IM*, the fundamental period of vibration is calculated for each bridge model through eigenanalysis. The bridge models differ for the values of H/D and the local soil conditions. Therefore, also the *IM*s change from model to model.

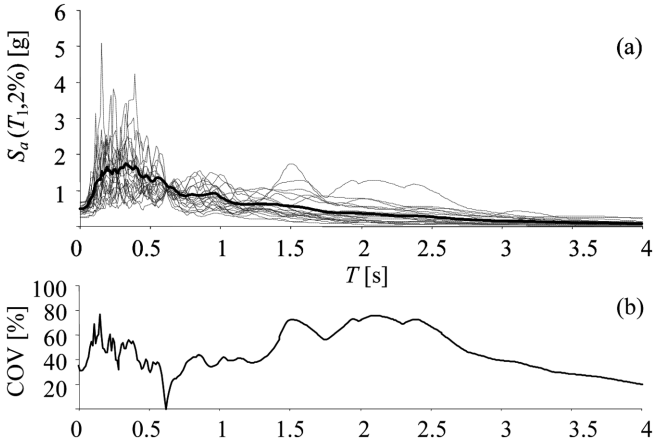

Fig. 5 Scaled pseudo-acceleration spectra for the model corresponding to H/D = 3 and ground type A: (a) individual record and average pseudo-accelerations, (b) coefficient of variation (COV) of pseudo-acceleration spectra

In the present study, for every value of H/D and for every ground type considered, a nonlinear multi-record IDA based on a set of 22 ground motion records is performed. Discrete values of the IM with a resolution of 0.1 g are used, covering the whole range of structural behavior from elastic to failure conditions. Global and intermediate EDPs are chosen to monitor the structural response. These $EDPs$ are the maximum absolute values, computed over the entire time history, of pier and abutments reactions, deck bending moments, and displacement of the center of the mass of the superstructure (referred as to control node hereinafter). For every value of the IM, the mean and the standard deviation of the response parameters of interest are calculated, allowing the estimation of the COV of each EDP. Failure conditions are reached when the mean values of the pier curvatures and/or of the deck transverse moments reach their capacity, whichever happen first.

The four sets of ground motions are selected from the PEER Database (PEER 2006). The following selection criteria are employed: (1) the shear wave velocity of the local soil at the site where the ground motion is recorded matches the assumed value with a tolerance of 50 m/s, (2) the source-to-site distance is assumed in the range between 25 and 75 km, and (3) the earthquake magnitude, M, is assumed in the range from 5.5 to 7.5. Since this study focuses only on the transverse direction, the two orthogonal horizontal components of each ground motion of the database are applied independently in a single-record IDA. The complete list of the selected ground motions can be found in Tubaldi *et al.* (2009). The ground motions have been normalized so that $S_a(T_1, \xi)$ is equal for all records in correspondence of the model natural period, T_1, and equivalent viscous damping ξ = 2%. Other features of the earthquake ground motions, such as frequency content and ground motion duration, are not modified by the scaling procedure adopted in this paper.

It is noteworthy that the analyzed bridge models are characterized by different natural periods of vibration, each corresponding to a different H/D value. Thus, a different set of normalized input ground motions must be employed for each model characterized by a different H/D value. Due to space constraints, only selected results are shown here. Fig. 5(a) shows the normalized pseudo-spectral acceleration values as functions of the period T for the ground motions selected for local soil condition A and the model characterized by a value of H/D = 3. The grey lines refer to the

individual spectra, while the black thick line corresponds to the average value of the $S_a(T_1, \xi = 2\%)$. Fig. 5(b) shows the COV of the normalized spectra as a function of the period T for the model with $H/D = 3$ and ground type A. The COV is equal to zero for $T = T_1$ and assumes relatively high values (up to 80%) for other periods. The results of multi-record IDA, which are based on nonlinear time history analyses (NTHAs), are compared with the results of linear time history analysis (LTHA) with earthquake base excitations defined by the same normalized ground accelerations used in the NTHA. This study requires performing more than 15000 NTHAs. The LTHA results for all IM values are obtained by scaling the results obtained via a single time history analysis of the linear elastic FE model. Ad-hoc pre-processor and post-processor routines have been implemented in Matlab (Math Works 1997), in order to perform the FE dynamic analyses in OpenSees and post-process the obtained analysis results using parallel computation (Vamvatsikos 2007) on a computer cluster comprising 104 central processing units.

6. Eigenanalysis results

The periods of vibration and the corresponding elastic modal shapes for the undamped FE models of the bridges are obtained through eigenanalysis for all the seven values of slenderness ratio H/D and the four ground types considered in this study.

Fig. 6 shows the modal shapes for vibration modes 1 and 3 corresponding to $H/D = 3$ and ground type A. These two modes are associated to the highest participating mass in the transverse direction. The second mode of vibration corresponds to an antisymmetric vibration shape with zero

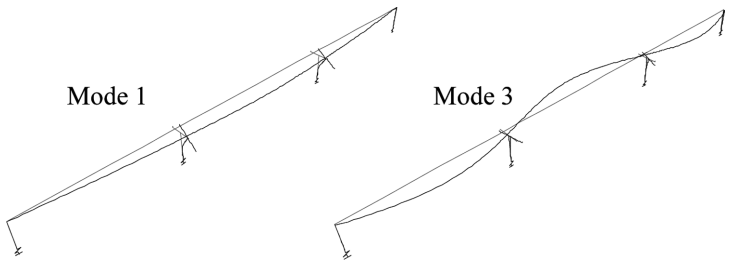

Fig. 6 Bridge modal shapes corresponding to vibration modes 1 and 3 in the transverse direction ($H/D = 3$, ground type A).

Table 4 Periods of first and third modes of vibration

	T_1					T_3			
H/D	A	B	C	D	*H/D*	A	B	C	D
3	0.623	0.630	0.639	0.663	3	0.173	0.175	0.182	0.257
4	0.838	0.843	0.850	0.868	4	0.174	0.176	0.183	0.256
5	1.016	1.020	1.025	1.039	5	0.174	0.176	0.183	0.256
6	1.157	1.160	1.164	1.176	6	0.174	0.176	0.183	0.256
7	1.260	1.262	1.266	1.276	7	0.174	0.177	0.184	0.256
8	1.339	1.341	1.345	1.354	8	0.175	0.177	0.184	0.256
9	1.402	1.404	1.407	1.416	9	0.175	0.177	0.184	0.256

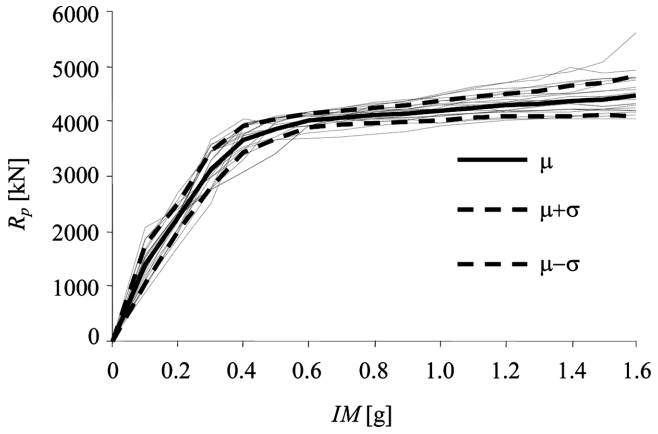

Fig. 7 Multi-record IDA: pier reactions (H/D = 3, ground type A)

participating mass and, thus, is not shown here.

The values of the periods corresponding to vibration modes 1 (T_1) and 3 (T_3) for all models developed are summarized in Table 4. The period elongation induced by the SSI effects is very small for ground types A, B and C, while it is more evident for ground type D, particularly for vibration mode 3. The results of these eigenanalyses are employed to define the *IM* and the normalized ground motion records used in the multi-record IDAs for both nonlinear hysteretic and linear elastic FE models.

7. Mean and variance of the structural response considering record-to-record variability

The uncertainty in the structural response induced by record-to-record variability can be efficiently described by the first- and second-order statistical moments of the multi-record IDA results. A meaningful representation of the uncertain structural response for different levels of the *IM* requires accurate estimates of the mean and standard deviation of the *EDP*s of interest. In particular, the sample standard deviation of the *EDP*s can be used to estimate confidence intervals for the *EDP* sample mean under appropriate hypotheses on the *EDP* distribution. The results of the multi-record IDA corresponding to H/D = 3 and ground type A are presented here and discussed in detail. The interested readers are referred to Tubaldi *et al.* (2009) for additional detailed results.

Fig. 7 plots the pier reactions, R_p, for increasing values of the seismic intensity measure *IM*. The thin grey lines represent the response for the different input ground motions. The black solid line represents the mean response (estimated as sample mean of the maximum response values recorded over the entire response time histories of each IDA performed), while the black dashed lines correspond to the mean ± one standard deviation (estimated as sample standard deviation of the maximum response values recorded over the entire response time histories of each IDA performed) of the response. Yielding of the piers takes place at *IM* = 0.40 g. For larger values of *IM*, extensive inelastic behavior is observed until failure is reached at *IM* = 1.60 g due to the exceedence of the pier curvature capacity. The dispersion of R_p, measured by its COV, is significant for low values of the intensity (e.g., COV = 0.25 for *IM* = 0.20 g) and decreases for increasing values of *IM* (e.g., COV = 0.08 for *IM* = 1.60 g). This phenomenon can be explained observing that the pier reactions

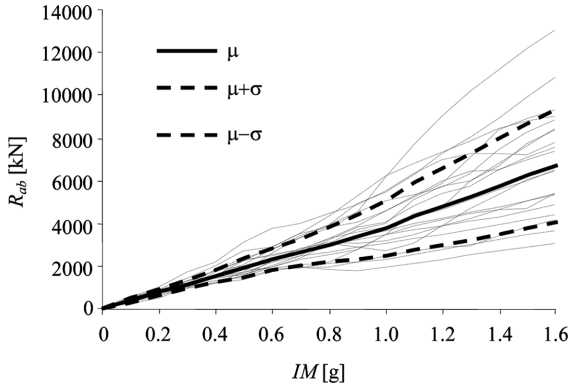

Fig. 8 Multi-record IDA: abutment reactions (H/D = 3, ground type A)

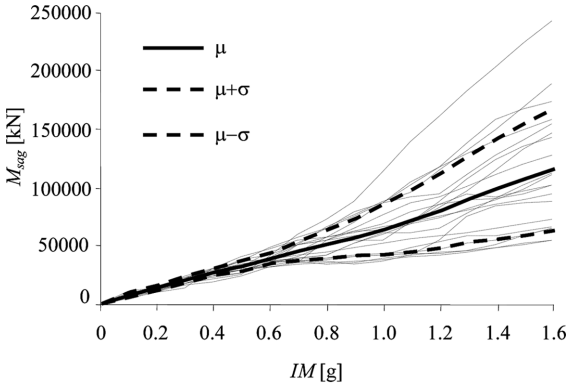

Fig. 9 Multi-record IDA: transverse moments at midspan of the center span (H/D = 3, ground type A).

at yielding/failure are mainly dependent on the pier yielding/ultimate moments. These quantities are only slightly influenced by the record-to-record variability (through the bending moment-axial force interaction captured by the fiber-section model used in the plastic hinge zones and through the change in the shear force distribution at the piers due to higher modes effects), since the structural system (and thus the capacity of the structural components) is modeled as deterministic.

Figs. 8 and 9 provide abutment reactions (R_{ab}), and transverse bending moments at midspan (M_{sag}) as functions of IM. The abutment reactions increase almost linearly for $IM \leq 1.0$ g. For $IM > 1.0$ g, the abutment reactions increase with a slightly higher rate, due to yielding of the piers and consequent transmission of inertia forces to the abutment reactions. A similar rate increase is also observed for M_{sag}, even if less pronounced than for R_{ab}. The COVs of both R_{ab} and M_{sag} increase for increasing value of IM, reaching significantly large values at failure conditions. In particular, the COV of R_{ab} increases from 0.24 at IM = 0.1 g to 0.39 at failure (IM = 1.60 g), and the COV of M_{sag} increases from 0.25 at IM = 0.1 g to 0.46 at IM = 1.60 g.

For a useful statistical description of the considered EDPs, a measure of the accuracy with which the mean response is estimated by the multi-record IDA is also needed. In this study, this measure of accuracy is provided by the coefficient of variation of the statistical estimator of the mean response (denoted here as $c.o.v._{EDP}$). Assuming statistical independence of the samples, $c.o.v._{EDP} \approx \mathrm{COV}/n^{0.5}$, in which n denotes the number of input ground motions considered. For the EDPs considered, $\max(c.o.v._{EDP}) = c.o.v._{M_{hog}} = 0.117$, in which M_{hog} = transverse moment evaluated at the hogging regions. The obtained low values of $c.o.v._{EDP}$ suggest that the results presented are quite accurate. It is noteworthy that the models corresponding to $H/D > 3$, not shown here due to space constraints, tend asymptotically to a linear elastic behavior and are characterized by a lower dispersion of the results than for the case with H/D = 3 (Tubaldi e*t al.* 2009).

8. Influence of *H/D* on the mean response

The values of the EDPs of the bridges considered are strongly dependent on the parameter H/D. Due to space constraints, only the cases corresponding to the two extreme values H/D = 3 and 9 are presented and discussed here. It is noteworthy that the bridges corresponding to H/D = 4 through 8

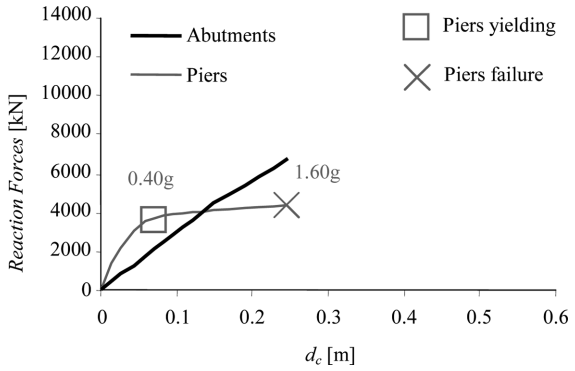

Fig. 10 Reaction forces at abutments and piers vs. control node displacement for *H/D* = 3 and ground type A

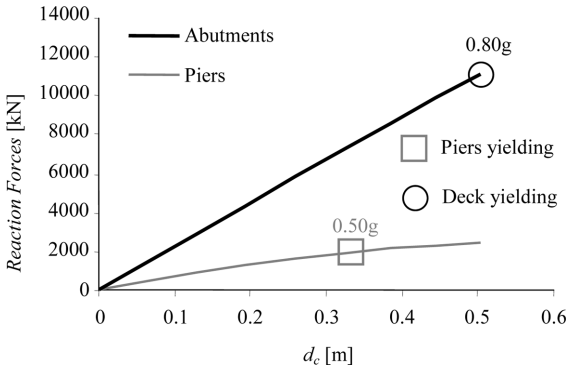

Fig. 11 Reaction forces at abutments and piers vs. control node displacement for *H/D* = 9 and ground type A

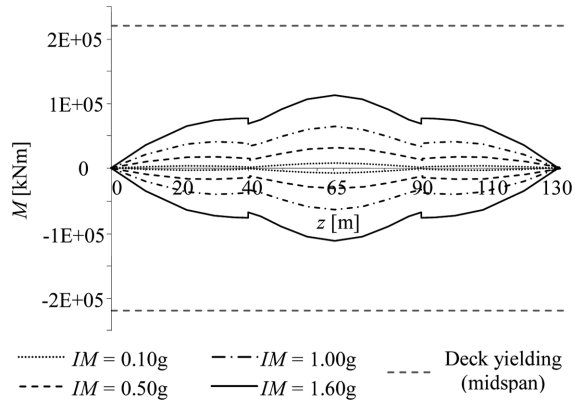

Fig. 12 Transverse bending moments for increasing values of *IM* for *H/D* = 3 and ground type A

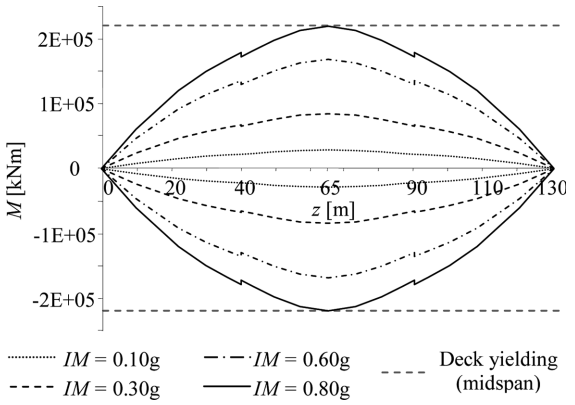

Fig. 13. Transverse bending moments for increasing values of *IM* for *H/D* = 9 and ground type A

present intermediate behaviors between those bridges with *H/D* = 3 and 9.

Global dynamic pushover curves corresponding to ground type A are plotted in Fig. 10 for *H/D* = 3 and in Fig. 11 for *H/D* = 9, respectively. The pier reactions-control node displacement curves represent the inelastic load path, while the abutment reactions-control node displacement curves correspond to the elastic load path for the considered structural system. For *H/D* = 3 and at low values of *IM*, the stiffness of the piers is relatively high compared to the deck-abutments system stiffness and large seismic forces are transferred to the piers and their foundations. For *IM* = 0.40 g, the piers exhibit inelastic flexural behavior at their base and their reaction forces are limited by the pier moment capacity. As a result, the seismic load path involving abutments (i.e., the elastic load path) becomes increasingly important for higher values of *IM*. Piers reach their ultimate curvature before the deck yields for *IM* = 1.60 g, corresponding to an average *PGA* = 0.70 g. The average *PGA* is calculated as the sample mean of the *PGA*s of the ground motions scaled to have the same *IM* value. This alternative measure of the seismic intensity is also reported because it is often considered as an important quantity for the design of a bridge.

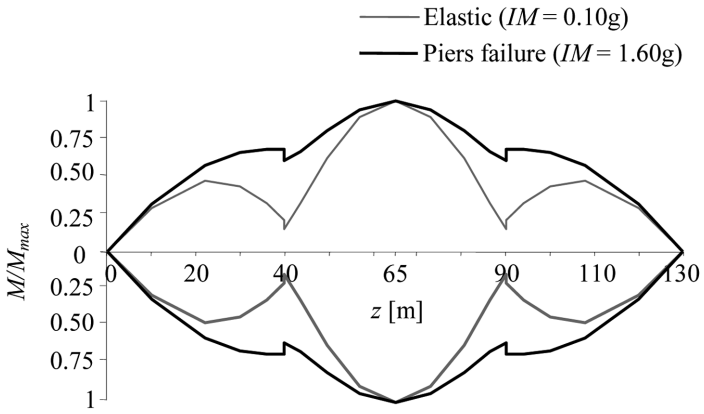

Fig. 14 Normalized transverse bending moment diagrams for H/D = 3

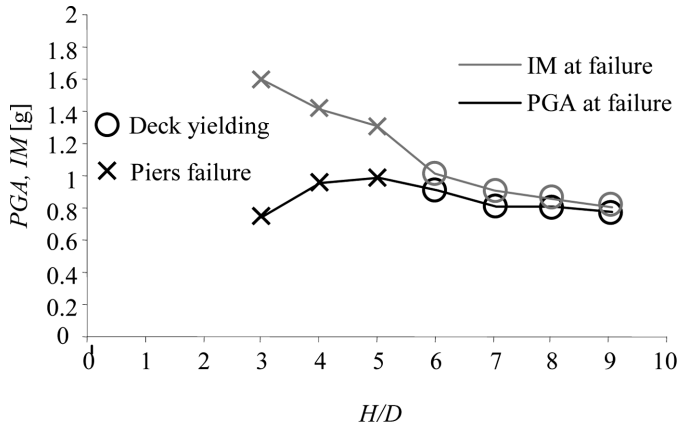

Fig. 15 Ultimate IM and PGA versus slenderness H/D for the bridge models corresponding to ground type A

In the case H/D = 9, piers are relatively very flexible compared to the deck-abutments system and yield for IM = 0.50 g (average PGA = 0.49 g). Failure of the system is reached for IM = 0.80 g (average PGA = 0.78 g) due to yielding of the deck at the midspan of the center span, before the piers reach their ultimate curvature. The response at the abutments is almost linear in all the cases considered.

Figs. 12 and 13 show the evolution of the moment diagrams for increasing values of the IM as functions of the deck cross-section coordinate along the longitudinal axis for H/D = 3 and 9, respectively. The moment demand at the critical cross-section (i.e., midspan of the central span) is also compared with the corresponding yield moment (moment capacity). For the case H/D = 3 (Fig. 12), the superstructure moments at ultimate condition are lower than the yield moment of the deck. For the case H/D = 9 (Fig. 13), the moment distribution is only slightly influenced by the presence of the piers. Failure is attained when the maximum bending moment acting on the deck reaches the yield value at the critical cross-section.

Fig. 14 highlights the variation of the shape of the transverse bending moment diagram along the longitudinal axis of the deck for the case H/D = 3. The bending moments are normalized by

dividing them by their maximum value. The normalized bending moments are plotted for IM = 0.10 g (thin grey line, corresponding to elastic behavior), and for IM = 1.60 g (thick black line, corresponding to failure). In this case, the two normalized bending moment diagrams are very different. It is noteworthy that the two normalized bending moment diagrams present increasingly smaller differences for increasing values of H/D and almost coincide for H/D = 9.

Fig. 15 shows the maximum values of the IM that the bridge can withstand up to failure as a function of H/D. The same figure plots also the values of the average PGA corresponding to the ultimate IMs. A large variation of the ultimate IM and PGA is observed for the different H/D values. The IM at failure is always decreasing for increasing values of the slenderness. The average PGA slightly increases for increasing slenderness of the piers with $H/D \leq 5$, corresponding to the flexural failure of the piers. For $H/D > 5$, corresponding to the attainment of the deck moment capacity, the average PGA decreases for increasing H/D due to the reduction of the energy dissipation promoted by the pier yielding. The maximum value of ultimate PGA is attained when the pier failure occurs together with the deck yielding (balanced failure). In this specific case, the maximum value of ultimate PGA is equal to 0.97 g and is reached for H/D = 5.

9. Influence of ground type on the response

SSI effects can influence significantly the seismic response of structural systems (Ciampoli and Pinto 1995, Jeremic *et al.* 2004, Zhang *et al.* 2008). In particular, for the bridge typology considered in this study, SSI can manifest itself through the following effects (referred to as SSI-only effects hereinafter): (1) SSI-induced abutment displacements, which can reduce the deck curvature and increase pier displacement demand, (2) SSI-induced pier displacements, which can reduce the pier curvature demand (Ciampoli and Pinto 1995), (3) introduction of additional sources of damping, and (4) elongation of the periods of vibration.

In addition to SSI-only effects, the seismic response of the considered bridges is significantly

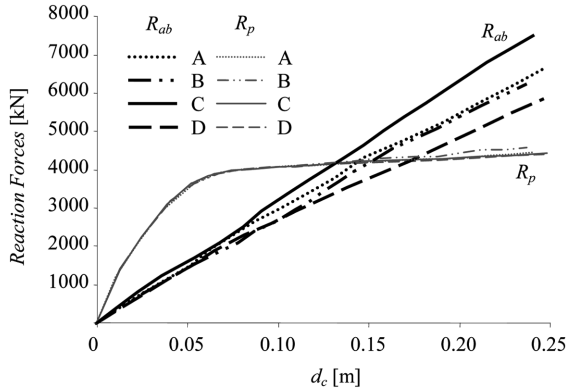

Fig. 16 Dynamic pushover curves for the FE model corresponding to H/D = 3 and ground type A, subjected to the four different set of input ground motions (i.e., corresponding to the different soil types considered)

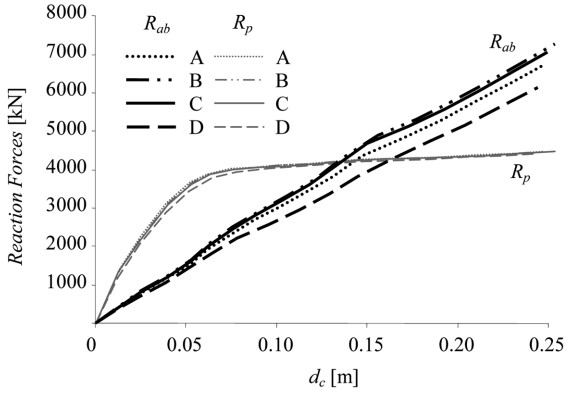

Fig. 17 Dynamic pushover curves for the FE models corresponding to H/D = 3 and different ground types, subjected to the set of input ground motions corresponding to soil type A

dependent on the frequency content of the input ground motions (frequency content effects). This frequency content is very different among the four sets of ground motion records corresponding to the four different ground types included in the performed parametric study. For every value of the pier slenderness H/D, four models have been analyzed, each corresponding to a different ground type. Due to space constraints, only selected results for the FE models corresponding to $H/D = 3$ are presented here, while general considerations are provided based on all available results.

In order to evaluate the sensitivity of the seismic response to the frequency content effects only, the bridge models for all values of H/D and corresponding to ground type A (rock or very stiff soil) have been subjected to the four different set of ground motions. For $H/D = 3$, the mean values of R_{ab} are characterized by a significant variability, while the pier reactions R_p show a very limited variability (Fig. 16). These different behaviors can be explained based on the effects of pier yielding on the local and global structural behavior: (1) locally, pier yielding directly limits the dispersion of the pier reactions (deterministic moment capacity), and (2) globally, pier yielding produces an elongation of the natural period of the structure. This second phenomenon, combined with the higher modes effects, increases the variability of the abutment reactions, since the input ground motions are normalized in correspondence of the natural vibration period of the undamaged structure and, thus, present a larger dispersion for any other period (Fig. 5(b)). It is observed that the third mode of vibration has a non-negligible influence on the abutment reactions and a very small influence on the pier reactions. For increasing H/D, the dispersion due to different frequency content of the input ground motions of both pier and abutment reactions reduces significantly and is almost negligible for $H/D = 9$.

In order to investigate the influence of the SSI-only effects, the bridge models for all values of H/D and all four different local soil types considered have been subjected to the same set of ground accelerations, corresponding to ground type A. The estimated mean responses of piers and abutments for the models with $H/D = 3$ are represented in terms of dynamic pushover curves in Fig. 17. For the models with $H/D = 3$, pier reactions (R_p) are only slightly influenced by the local soil type while abutment reactions (R_{ab}) are increasingly influenced by the local soil type for increasing values of IM. This phenomenon is induced by the period elongation due to both SSI effects and pier plasticization and by higher modes effects. For increasing values of H/D, the dispersion of both R_p and R_{ab} due to SSI-only effects reduces significantly and is almost negligible for $H/D = 9$.

It is observed that, for this specific soil-structure system, the frequency content effects have a larger influence on the mean values of R_p and, in particular, of R_{ab} than SSI-only effects. The combination of SSI-only and frequency content effects is very small on the pier reactions and significant on the abutment reactions. These effects decrease for increasing values of H/D, i.e., when the structures exhibit only a moderate nonlinear behavior. The influence of the ground type on the failure condition of the structural systems does not have a monotonic trend (i.e., in some cases SSI is detrimental, in others beneficial) in terms of maximum value of IM, which is consistent with results available in the literature (Jeremic *et al.* 2004, Mylonakis and Gazetas 2000).

10. Comparison between analysis results corresponding to elastic and inelastic models

Several design procedures suggested in modern seismic design codes are based on linear elastic analyses coupled with the use of a response spectrum modified by a reduction factor. This reduction factor accounts for the fact that the seismic loads acting on the actual structure are smaller than the

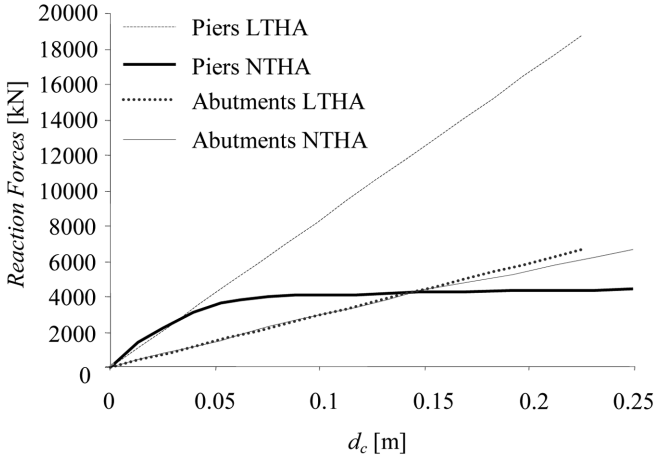

Fig. 18 Comparison between LTHA and NTHA results: dynamic pushover curves for H/D = 3 and ground type A

loads that would act on the same structure if it remained linear elastic. In this paper, in order to evaluate the suitability of simplified linear elastic analyses often accepted by modern design codes in estimating the actual structural behavior of SCC bridges, the results of nonlinear multi-record IDAs (NTHA) are compared with the results obtained by time history analysis (LTHA) performed on the linear elastic FE models of the bridges for increasing values of the seismic intensity measure (*IM*). Due to space constraints, only selected results are presented here.

In Fig. 18, the reaction forces at the piers and abutments are plotted as functions of the control node displacement d_c (elastic and inelastic dynamic pushover curves) for the model corresponding to H/D = 3 and ground type A. Piers exhibit an extensive inelastic behavior and, thus, the maximum pier reactions evaluated by LTHA are very different from the corresponding values obtained through NTHA. The ratio between linear and nonlinear pier reaction forces, r_p, is equal to 4.22 at failure. The abutment reaction forces provided by LTHA are very close to the values provided by NTHA for all considered seismic intensity values. For increasing values of H/D, the discrepancy between LTHA and NTHA results reduces, since the structural system experiences smaller inelastic deformations.

Figs. 19 and 20 provide the ratios between the maximum values of different *EDP*s (i.e., pier/abutment reactions and transverse bending moments monitored at the sagging/hogging regions, respectively) obtained through LTHA and NTHA, as functions of the slenderness H/D for all different ground types considered in this study. For every selected ground motion record, the maximum value of each *EDP* of interest provided by LTHA is divided by the corresponding value provided by NTHA, evaluated at the failure condition. For all considered *EDP*s, four curves are generated, each corresponding to a single set of ground motion records (i.e., corresponding to a different ground type). Each point of these curves is obtained for different values of H/D by averaging the *EDP* ratios corresponding to all ground motion records of the relative set.

Fig. 19 provides the elastic-to-inelastic ratios of pier ($r_p = R_{p(\mathrm{LTHA})}/R_{p(\mathrm{NTHA})}$) and abutment ($r_{ab} = R_{ab(\mathrm{LTHA})}/R_{ab(\mathrm{NTHA})}$) reactions for the different values of H/D. The ratio r_p assumes values between 3.86 and 5.43 for H/D = 3 (when the failure corresponds to achievement of the pier moment demand) and significantly decreases for increasing slenderness, reaching values between 1.26 and 1.35 for H/D = 9 (when the failure corresponds to deck yielding). On the other hand, r_{ab} assumes

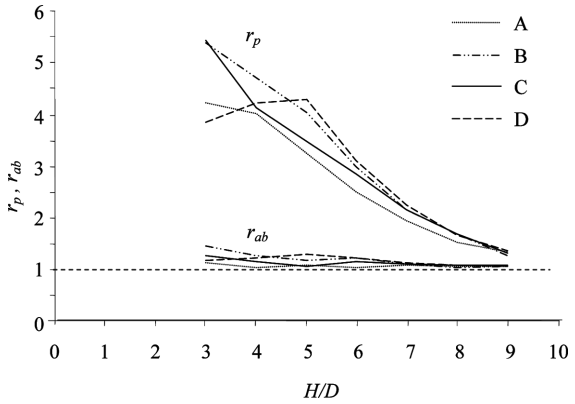

Fig. 19 Elastic-to-inelastic ratio of pier and abutment reaction forces

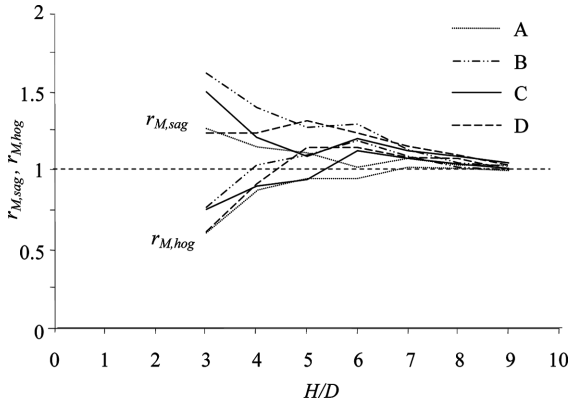

Fig. 20 Elastic-to-inelastic ratio of transverse deck moments

values close to one (between 1.03 and 1.44) for all considered values of pier slenderness and for all ground types.

Fig. 20 shows the elastic-to-inelastic ratios of deck bending moments at the midspan of the central span, $r_{M,sag}$, and at the supports, $r_{M,hog}$. The values of $r_{M,sag}$ are always larger than one, vary between 1.01 and 1.61, and in general decrease for increasing values of H/D. The values of $r_{M,hog}$ present a more complex non-monotonic trend: $r_{M,hog}$ are smaller than one for small slendernesses (e.g., for $H/D = 3$, $r_{M,hog}$ varies between 0.60 and 0.76), increase for intermediate slendernesses, and tend (asymptotically) to one for large values of H/D (e.g., for $H/D = 9$, $r_{M,hog}$ varies between 0.99 and 1.01). It is noteworthy that values $r_{M,hog}$ smaller than one indicate that LTHA underestimates the transverse bending moments in the hogging regions (i.e., at the supports provided by the piers). The elastic-to-inelastic ratios of the control node displacements, r_d, follow a trend similar to $r_{M,sag}$ and, in general, assume values larger than one, particularly for small values of H/D.

It is noteworthy that current design codes define a global strength reduction factor (also called behavior factor) as the ratio of the elastic strength demand to the design (inelastic) strength demand (Elnashai and Di Sarno 2008). For structural systems such as common frames and other systems that can, in general, be approximately modeled as elastic-perfectly plastic single-degree-of-freedom systems, the strength reduction factor, R, is given by the product of the elastic-to-inelastic ratio of the total base shear demand, R_μ, and the overstrength factor, Ω_d (Elnashai and Di Sarno 2008), i.e., $R = R_\mu \cdot \Omega_d$. This definition can be applied also to bridges without abutment restraints, in which only one (inelastic) load path can be identified and $R_\mu = r_p$. However, for the structural system considered herein, the results shown in Figs. 19 and 20 suggest that an approach based on (global or partial) strength reduction factors is not appropriate for this specific system exhibiting dual load path behavior. This conclusion can be explained by the fact that r_p changes drastically for different values of H/D and different local soil conditions, particularly for large values of H/D, for which the deck yielding condition prevents the slender piers to undergo large inelastic deformations. In addition, for small H/D, $r_{M,hog} < 1$ indicates that a linear elastic analysis would significantly underestimate the bending moments acting on the hogging regions.

In addition to the mean values of the *EDP* ratios previously discussed, the standard deviations and coefficients of variation of the *EDP* ratios are also calculated for each ground type and H/D value. It is found that the ratios of the *EDP*s of interest are characterized by very high coefficient of

variations, ranging from 56% for the short piers case to 10% for the slender piers case. This implies that, for specific ground motions, the actual elastic-to-inelastic ratios of the considered *EDP*s computed when the structural systems reach failure can significant deviate from the average values shown in Figs. 19 and 20 and previously discussed.

11. Conclusions

This study focuses on assessing the influence of piers-deck stiffness ratio and soil-structure interaction on the post-elastic seismic behavior of continuous steel-concrete composite bridges with dual load path behavior. Advanced nonlinear finite element models of a typical bridge configuration for different height-to-diameter (*H/D*) ratios of the piers and different local soil conditions are developed using the simulation software framework OpenSees. Nonlinear multi-record incremental dynamic analysis (IDA) is employed to evaluate mean and standard deviation of pertinent engineering demand parameters (*EDP*s) for different values of the intensity measure (*IM*). The results obtained through nonlinear multi-record IDA are also compared with those obtained by using multi-record linear time history analyses. Based on the results of the analyses, the following observations are made:

(1) All monitored *EDP*s are very sensitive to the variation of the deck-to-piers relative stiffness, modeled through the variation of the pier slenderness *H/D*. The failure mechanism switches from a pier flexural failure mechanism for short piers ($H/D \leq 4$) to a deck yielding mechanism for tall piers ($H/D \geq 5$). The seismic input variability induces a limited dispersion in the pier reactions, which are mainly dependent on the deterministic pier yielding/ultimate moments. On the contrary, the monitored *EDP*s related to the components involved in the linear load path (i.e., abutment reactions, deck transverse displacements and bending moments) are characterized by larger dispersions.

(2) The local soil conditions influence moderately the seismic behavior of the analyzed bridges, through soil-structure interaction effects and different frequency content of the ground motion records. Higher modes of vibration affect significantly the response of the abutments.

(3) The elastic-to-inelastic ratios of pier reactions significantly decrease for increasing values of the pier slenderness *H/D*. This phenomenon is due to the constraint imposed by the yielding condition of the deck, which prevents the piers from undergoing large inelastic deformations. A weaker dependency on *H/D* is observed for the elastic-to-inelastic ratios of the abutment reactions. These ratios always assume values close to one. Elastic-to-inelastic transverse bending moments ratios are always higher than one in the sagging regions. At the hogging regions these moment ratios assume values smaller than one for the models with stiff piers and tend asymptotically to one for increasing *H/D*.

(4) A simplified analysis approach based on linear elastic analysis and a global strength reduction factor, while often accepted in modern seismic codes, is found inappropriate for this specific system showing dual load path behavior. In fact, the transverse bending moments acting on the deck can significantly be underestimated by linear analysis procedures, in the case of high piers-to-deck stiffness ratios (i.e., small values of *H/D*). However, for small values of piers-to-deck stiffness ratios (i.e., large values of *H/D*), the deck yielding condition becomes dominant and the use of a strength reduction factor is not justified, since the piers cannot provide inelastic dissipation of the seismic load energy.

Acknowledgements

The authors gratefully acknowledge partial support of this research by the Louisiana Board of Regents through the Pilot Funding for New Research (Pfund) Program of the National Science Foundation (NSF) Experimental Program to Stimulate Competitive Research (EPSCoR) under Award No. NSF (2008)-PFUND-86. Opinions expressed in this study are those of the authors and do not necessarily reflect those of the sponsor.

References

Astaneh-Asl, A., Bolt, B., Mcmullin, K.M., Donikian, R.R., Modjtahedi, D. and Cho, S.W. (1994), "Seismic performance of steel bridges during the 1994 the Northridge earthquake", Report. no. UCB/CE-Steel- 94/01. Dept. of Civil Engineering, Univ. of California, Berkeley, CA.

Aviram, A., Mackie, K.R. and Stojadinovic, B. (2008), "Effect of abutment modeling on the seismic response of bridge structures", *Earthq. Eng. Eng. Vib.*, **7**(4), 395-402.

Benzoni, G., Limongelli, M.P. and Priestley, M.J.N. (2003), "Assessment of shear forces on bridge abutments. A simplified method", *J. Bridge Eng.*, **8**(1), 29-38.

Calgaro, J.A. (1994), *Conception des ponts*, Presses de l'Ecole nationale des ponts et chaussées (ENPC), Paris.

California Department of Transportation (Caltrans) (2006), *Seismic Design Criteria 1.4*, Caltrans Division of Structures, Sacramento, California.

Calvi, G.M. (2004), "Recent experience and innovative approaches in design and assessment of bridges", *Proceedings of 13th World Conference on Earthquake Engineering*, Vancouver, August.

Chopra, A.K. (2001), *Dynamics of structures: Theory and Applications to earthquake engineering*, 2nd Edition, Prentice Hall, Englewood Cliffs, N.J.

Ciampoli, M. and Pinto, P.E. (1995), "Effects of soil-structure interaction on inelastic seismic response of bridge piers", *J. Struct. Eng-ASCE*, **121**(5), 806-814.

Dall'Asta, A. and Zona, A. (2002), "Non-linear analysis of composite beams by a displacement approach", *Comput. Struct.*, **80**(27), 2217-2228.

Dezi, F., Carbonari, S. and Leoni, G. (2009), "A model for the 3D kinematic interaction analysis of pile groups in layered soils", *Earthq. Eng. Struct. D.*, **38**(11), 1281-1305.

Dezi, L. (2008), "Architectural and structural design of short and medium span composite bridges", *Proceedings of 7th International Conference on Steel Bridges*, Guimaraes, Portugal.

Dezi, L. and Formica, M. (2006), "Impalcato bitrave a sezione composta. Verifica secondo gli Eurocodici", Strutture composte: nuove costruzioni, recupero, ponti, CISM, Italy.

Elnashai, A.S. and Di Sarno, L. (2008), *Fundamentals of Earthquake Engineering*, Wiley and Sons.

European Committee for Standardization (ECS) (2005), *Eurocode 8 - Design of structures for earthquake resistance*, EN1998, Brussels.

Lessloss-Risk Mitigation for Earthquakes and Landslides Integrated Project (2007), "Guidelines for displacement-based design of building and bridges", LESSLOSS Report No. 2007/05, IUSS Press, Pavia, Italy.

Itani, A.M., Bruneau, M., Carden, L. and Buckle, I.G. (2004), "Seismic Behavior of Steel Girder Bridge Superstructures", *J. Bridge Eng.*, **9**(3), 243-249.

Jeremic, B., Kunnath, S. and Xiong, F. (2004), "Influence of soil–foundation–structure interaction on seismic response of the I-880 viaduct", *Eng. Struct.*, **26**(3), 391-402.

Karsan, I.D. and Jirsa, J.O. (1969), "Behavior of concrete under compressive loading", *J. Struct. Div.*, **95**(12), 2543-2563.

Kawashima, K. (2007), "Seismic Damage in the Past Earthquakes, Seismic Design of Urban Infrastructure", http://seismic.cv.titech.ac.jp/en/lecture/seismic_design/.

Kent, D.C. and Park, R. (1971), "Flexural members with confined concrete", *J. Struct. Eng-ASCE*, **97**(7), 1969-1990.

Kolias, B. (2008), "Eurocode 8 – part 2. Seismic design of bridges", Eurocodes: Background and applications workshop, February, Brussels.
Mackie, K. and Stojadnovic, B. (2001), "Probabilistic Seismic Demand Model for California Highway Bridges", *J. Bridge Eng.*, **6**(6), 468-481.
Mackie, K. and Stojadnovic, B. (2005), "Fragility basis for California highway overpass bridge seismic decision making", PEER Report 2005/02, College of Engineering, University of California, Berkeley.
Mander, J.B., Priestley, M.J.N. and Park, R. (1988), "Theoretical stress-train model for confined concrete", *J. Struct. Eng-ASCE*, **114**(8), 1804-1826.
Math Works Inc. (1997), *Matlab - High performance numeric computation and visualization software*, *User's guide*, Natick, MA, USA.
McKenna, F., Fenves, G.L. and Scott, M.H. (2006), "OpenSees: Open system for earthquake engineering simulation", Pacific Earthquake Engineering Center, University of California, Berkeley, CA., http://opensees.berkeley.edu/.
Menegotto, M. and Pinto, P.E. (1973), "Method for analysis of cyclically loaded reinforced concrete plane frames including changes in geometry and non-elastic behavior of elements under combined normal force and bending", *Proceeding of IABSE Symposium*, Lisbon, Portugal.
Mwafy, A.M. and Elnashai, A.S. (2001), "Static pushover versus dynamic collapse analysis of RC buildings", *Eng. struct.*, **23**(5), 407-424.
Mylonakis, G. and Gazetas, G. (2000), "Seismic soil–structure interaction: beneficial or detrimental?", *J. Earthq. Eng.*, **4**(3), 277-301.
Pacific Earthquake Engineering Center (PEER) (2006), "PEER strong motion database," http://peer.berkeley.edu/smcat.
Panagiotakos, T.B., Bardakis, V. and Fardis, M.N. (2006), "Displacement-based Seismic Design Procedure for Concrete Bridges with Monolithic Connection between Deck and Piers", *Proceedings of 2nd fib Congress*, Naples, Italy.
Priestley, M.J.N., Calvi, G.M. and Kowalsky, M.J. (2007), *Displacement-Based Seismic Design of Structures*, IUSS Press, Pavia, Italy.
Scott, M.H. and Fenves, G.L. (2006), "Plastic Hinge Integration Methods for Force-Based Beam-Column Elements", *J. Struct. Eng-ASCE*, **132**(2), 244-252.
Shome, N., Cornell, C.A., Bazzurro, P. and Carballo, J. (1998), "Earthquake, Records, and Nonlinear MDOF Responses", *Earthq. Spectra*, **14**(3), 469-500.
Tubaldi, E., Barbato, M. and Dall'Asta, A. (2009), "Parametric study of continuous steel-concrete composite bridges exhibiting dual load path", Technical Report, Department of Civil and Environmental Engineering, Louisiana State University and A&M College, Baton Rouge, LA.
Vamvatsikos, D. (2007), "Performing incremental dynamic analysis in parallel using computer clusters", *Proceedings of COMPDYN2007 Conference on Computational Methods in Structural Dynamics and Earthquake Engineering*, Rethymno, Greece.
Vamvatsikos, D. and Cornell, C.A. (2002), "Incremental dynamic analysis", *Earthq. Eng. Struct. D.*, **31**(3), 491-514.
Wolf, J.P. (1985), *Dynamic Soil–Structure Interaction*, Prentice-Hall, Englewood Cliffs, N.J.
Zona, A., Barbato, M. and Conte, J.P. (2008), "Nonlinear seismic response analysis of steel-concrete composite frames", *J. Struct. Eng-ASCE*, **134**(6), 986-997.
Zhang, J. and Makris, N. (2002), "Seismic response analysis of highway overcrossings including soil–structure interaction", *Earthq. Eng. Struct. D.*, **31**(11), 1967-1991.
Zhang, Y., Conte, J.P., Yang, Z., Elgamal, A., Bielak, J. and Acero, G. (2008), "Two-dimensional nonlinear earthquake response analysis of a bridge-foundation-ground system", *Earthq. Spectra*, **24**(2), 343-386.